



ELSEVIER

Contents lists available at ScienceDirect

Polymer Testing

journal homepage: www.elsevier.com/locate/polytestPOLYMER
TESTING

ROGER BROWN

Test Method

Development of the split-Hopkinson pressure bar technique for viscous fluid characterization

Amanda S. Lim^{a,b}, Sergey L. Lopatnikov^{a,c}, John W. Gillespie, Jr.^{a,b,c,*}^a Center for Composite Materials, University of Delaware, Newark, DE 19716, USA^b Department of Materials Science and Engineering, University of Delaware, Newark, DE 19716, USA^c Department of Civil and Environmental Engineering, University of Delaware, Newark, DE 19716, USA

ARTICLE INFO

Article history:

Received 14 May 2009

Accepted 5 August 2009

Keywords:

High rate evaluation

Hopkinson pressure bar

Newtonian fluids

Characterization

Squeeze flow

ABSTRACT

The split Hopkinson pressure bar (SHPB) technique has been employed to evaluate the dynamic squeeze flow behavior of viscous Newtonian fluids. In this paper, the conditions under which classic Hopkinson bar data analysis is applicable for fluid specimens are discussed in detail. Requirements include the development of a parabolic flow profile and associated pressure distribution across the specimen. The times required for these processes to occur are calculated and compared with the experimental timescale in order to establish a specimen design criterion for valid SHPB testing. To evaluate this design criterion, an isothermal squeeze flow model describing the behavior of a cylindrical fluid specimen which includes inertial forces is used to predict the experimental results for a model Newtonian fluid. Good agreement between the theory and the experiment is obtained for thin specimens (~ 1.0 mm) across a wide range of shear strain rates (over 10^5 s⁻¹). As a result of this study, the conditions under which valid SHPB experimental results may be obtained for a Newtonian fluid specimen are identified.

© 2009 Elsevier Ltd. All rights reserved.

1. Introduction

The Hopkinson bar experimental technique has been implemented over the last 50 years to characterize the dynamic mechanical behavior of a variety of solid materials, such as metals, ceramics, composites, polymers, etc. under high rate compression, tension, and torsion loadings [1]. This paper expands the capabilities of the split-Hopkinson pressure bar (SHPB) experimental technique to the high rate characterization of viscous fluids.

Traditional techniques capable of imparting high shear rates within a viscous fluid include capillary and rotational rheometry. Capillary rheometers achieve high shear strain rates ($>10^5$ s⁻¹) at very high shear strains and medium to low shear stresses [2]. While highly effective for viscous

polymer melts, this technique has limitations for complex fluids (i.e. shear thickening fluids), as clogging of the capillary can occur.

Rotational rheometers achieve lower shear rates; however, recent efforts have been made to augment their capabilities by Lee and Wagner [3]. As a result, a ARES rheometer has been modified to achieve shear rates over 10^4 s⁻¹ in medium viscosity materials (~ 1 Pa s). While these techniques are capable of high shear rates at a moderate stress range, the Hopkinson pressure bar can achieve very high stresses, only limited by the yield stress of the bar material. Moreover, while rotational and capillary rheometers provide steady flow measurements, the SHPB is a dynamic experimental technique capable of measuring the transient response of a material to loading rate. This is especially important for complex fluids and suspensions which are rate sensitive.

Recently, modifications to the split-Hopkinson pressure bar technique have been made to accommodate the evaluation of fluids undergoing pure compression. Previously,

* Corresponding author. Center for Composite Materials, 201 Composites Manufacturing Science Laboratory, Newark, DE 19711, USA. Tel.: +1 302 831 8149.

E-mail address: gillespi@udel.edu (J.W. Gillespie Jr.).

Kenner [4] explored the propagation of stress waves through a column of fluid encased within a rigid tube. In their research, the Hopkinson bar technique was used to examine the dynamic behavior of glycerine and ethyl alcohol under pure compression. Kenner's work clearly defines requirements which must be met for the containing tube to be considered rigid and identifies testing conditions under which the classic one-dimensional transmission and reflection laws may be applied for fluids.

Hoglund and Larsson [5] and Åhrström et al. [6] later employed the split Hopkinson bar technique to investigate the behavior of elastohydrodynamic lubricants at high pressures. Their experimental setup is similar to that of Kenner's; however, their oil specimens were placed in a pre-stressed cemented carbide tube with a shrink-fit assembly of 5 rings of high-alloy steel which ensured that there was little or no radial expansion and thus no shear within the oil specimens during testing. A major difference between these two experimental setups is that the fluid column in Kenner's experiments is almost a meter long, while the specimens examined in the apparatus modified by Åhrström et al. are between 2 and 5 mm in length. Also, Kenner's experiments used a spherical projectile in lieu of the standard cylindrical striker bar. An important facet of the literature by Åhrström et al. is their identification of the timescale associated with wave propagation through a constrained fluid specimen. In this paper, we will expand this analysis to encompass the behavior of an unconstrained fluid undergoing dynamic squeezing flow.

The Hopkinson bar experimental method has also been used to study the behavior of viscous fluids under pure shear loading. Clyens et al. [7] employed the Hopkinson torsion bar to obtain high shear rate measurements of the viscosity of supercooled liquids. Later, the through bar method [8] was used to investigate the dynamic response of a high polymer silicon oil. In this technique, the oil surrounds the incident, or through bar, and is held in place by a coaxial cylinder, mimicking a Pochettino-type viscometer. During testing, the incident bar is driven through the fluid resulting in a pure shear loading. PMMA bars were used, making it possible to visually check that no air bubbles were present during testing. This use of viscoelastic bars adds a level of complexity to the SHPB data reduction. In addition, this method was not validated using a viscosity standard.

These innovative techniques have proven useful for evaluating the compressive and shear behavior of fluids separately. This study expands on these techniques by extending the traditional SHPB technique to characterize the high rate compression-induced shear response of a viscous fluid. In these experiments, the SHPB apparatus is used as a means of measuring the dynamic, high rate squeeze flow within a viscous fluid specimen. This technique allows for the evaluation of smaller volumes of fluid as well as for easier specimen loading. The aim of this study is two-fold: 1) quantify the experimental conditions and parameters required for valid SHPB evaluation of a Newtonian fluid specimen and 2) validate the test methodology and associated data reduction using known viscosity standards.

Two facets of SHPB data reduction for a viscous fluid are discussed. The first is related to the applicability of classic SHPB data reduction methodology to the case of a fluid

specimen. The second deals with establishing a relationship between the SHPB data (e.g. bar force and gap closing speed and acceleration) and the material properties of the fluid. Our approach is to first satisfy the classic force equilibrium assumptions, then to discuss further conditions which must be met for a fluid specimen to achieve the fully developed flow and pressure distributions derived for this test method (i.e. dynamic squeeze flow). The flow and pressure development times (referred to as characteristic times) are determined as a function of the specimen material properties and geometry. In order for the experiment to be valid, the duration of the test must be larger than the characteristic times required to achieve fully developed flow and pressure distribution conditions. A squeeze flow model which incorporates inertial effects is used to predict the experimental results of a model Newtonian fluid. Good correlation is seen for thin specimens (0.5–1.0 mm) that satisfy our test methodology. A criterion is derived to identify experimental conditions that will allow for accurate characterization of Newtonian fluids over a wide range of viscosities and strain rates.

2. Materials

The CANNON N4000 and N5100 Newtonian viscosity standards consist of 100% polybutene. An AR-G2 rotational rheometer was used to examine the shear rate dependence of these viscosity standards at 20 °C. The results for a continuous shear stress ramp are plotted in Fig. 1, where μ represents the dynamic viscosity of a Newtonian material and $\dot{\gamma}$ is the applied shear rate. At shear rates over 1000 s⁻¹, the power limits of the AR-G2 are reached and, as a result, the viscosity appears to drop drastically. This is not actual shear-thinning, but rather due to the power limits of the AR-G2. This follows standard rheological practice to show the limitations of the rheometer. From the rheological information in Fig. 1, it is clear that there is little or no rate dependent behavior for these specimens at shear rates up to 1000 s⁻¹. Thus, the N4000 and N5100 fluid specimens can be considered Newtonian at low to medium rates.

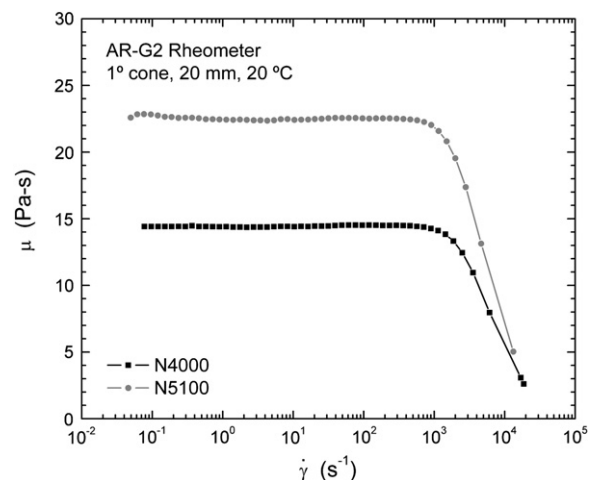


Fig. 1. Continuous shear–stress ramp of N4000 and N5100 at 20 °C. At approximately 1000 s⁻¹ the power limit of the AR-G2 is exceeded.

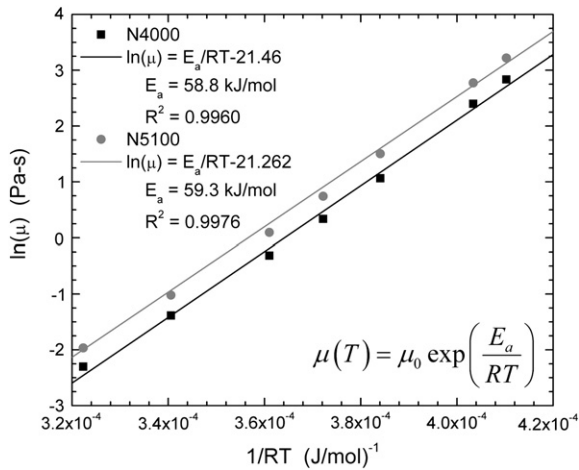


Fig. 2. Viscosity–temperature relationship for N4000 and N5100 standards.

The temperature dependence of the N4000 standard has been provided by CANNON and is plotted in Fig. 2. This data has been curve fitted and is used to determine the actual viscosity for each test, given the measured ambient temperature during testing. Here, E_a is the activation energy, R is the gas constant and T is the temperature of the specimen. While Fig. 2 shows a strong temperature dependence of these fluids, it should be noted that, experiments were performed at sufficiently low average shear rates to incur less than 1 °C temperature rise during testing.

A conservative estimate of the sound velocity of polybutene is 700 m/s [9] and will be used in estimating the characteristic timescales of the N4000 and N5100 fluid specimens. The density of the N4000 fluid is 883.2 kg/m³ (886.2 kg/m³ for N5100) at 20 °C. These values will be used in later analysis of the viscous fluid specimen behavior during SHPB testing.

3. Experimental

The diagram in Fig. 3 illustrates the SHPB experimental setup adapted for dynamic testing of viscous fluids. In the experiments discussed in this paper, the specimen and bar diameters are the same ($D_{SP} = D_{IB} = D_{TB}$). The aluminum (Alloy 6061-T651, $\sigma_y = 275.8$ MPa) bars used in these experiments were precision machined and centerless ground for a high degree of alignment. The bars are supported by four bearings to prevent bending and

maintain alignment. These bearings are machined to fit the bar outer diameter, resulting in reduced friction.

The fluid specimen is sandwiched between the bars and held in place by a soft, flexible band. A key and pin system was used to set the initial specimen thickness before each test (Fig. 4). Two pins were attached to the incident and transmission bars using strain gage adhesive. Several keys were machined to control the distance between the two pins. By using the keys to set the initial specimen thickness before testing, experimental data could be taken with a high degree of repeatability.

During each test, the flexible band encasing the fluid is stretched due to fluid expansion in the radial direction. This creates a force applied to the fluid from the band. An estimate of the magnitude of this effect was made using data from quasi-static tensile tests performed with an Instron 5567. It was determined that the modulus of the flexible band was ~1 MPa. Given the change in thickness during testing and considering conservation of fluid mass, the pressure developed by the band was negligible (two orders of magnitude lower) compared to the pressures developed during compression loading. No specimens were tested more than once in these experiments and a new band was used in each test.

Two strain gauges were mounted at the center of the incident and transmission bars at positions LSG-1 and LSG-2 from the IB-SP and SP-TB interfaces, respectively. The strain gauges are mounted on opposite sides of the bar and wired to cancel out radial strain, leaving only axial strain in the recorded data. At the beginning of each test, the striker bar is fired out of a 1 m long gas gun tube. Two infrared sensors, mounted 50.8 mm apart at the end of the tube, are used to measure the exit velocity of the striker bar, V_E , which is often used as a measure of comparison between different tests.

The striker bar impacts a pulse shaper, which is placed at the incident bar end. The pulse shaper material creates a near-triangular-shaped pulse which travels along the incident bar to the IB-SP interface. At this interface, a portion of the pulse is reflected while the rest passes through the specimen and along the length of the transmission bar. The factors affecting the magnitude of the reflected and transmitted pulses are the bar-specimen impedance (product of density, ρ , and wave speed, C_0) ratio and the geometric properties of the specimen. These experimental parameters, including the elastic modulus (E), are listed for each material in Table 1. The wave speed through each of the bars was determined through calibration experiments.

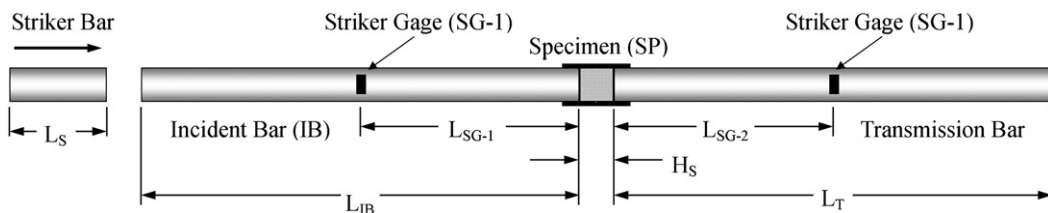


Fig. 3. SHPB experimental setup adapted from [11].

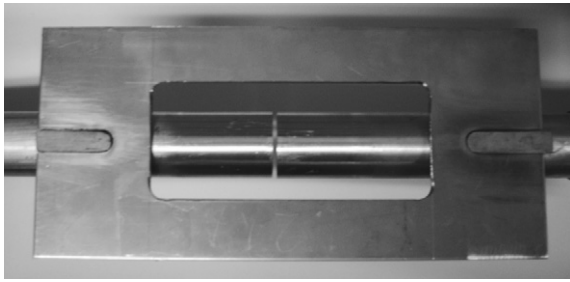


Fig. 4. Key and pin setup for specimen thickness control.

Several variables can be controlled in the test: the loading rate, the amplitude and the total duration of the incident pulse. The loading rate of the incident pulse was set using a cylindrical rubber pulse shaper (2.54 mm diameter, 1.45 mm thickness). This was found to yield the slowest loading rate possible while maintaining a clear distinction between the incident and reflected signals. Aluminum bars were used as their low impedance is sufficiently close match to the fluid without resorting to polymeric bars. The incident pulse amplitude was limited by the yield strength of the bars ($\sigma_y = 275.8$ MPa). The experiments reported in this paper were performed with maximum axial strain rates ($\dot{\epsilon}$) between 1000 s^{-1} (N4000) and 4000 s^{-1} (N5100) which induce shear rates, ($\dot{\gamma}$) between 46,000 and $175,000 \text{ s}^{-1}$. The loading times for these experiments range between 150 and $250 \mu\text{s}$. The transient material behavior is measured accurately within $0.2 \mu\text{s}$ intervals using a 5 MHz data acquisition rate.

4. Data reduction and analysis

4.1. Governing equations

The standard Hopkinson bar data reduction methodology presented by Grey [10] and discussed extensively by Gama [11] establishes the relationship between measured acoustic data and the force acting on the specimen as well as the specimen compression rate. The force applied to the specimen represents the average pressure distribution in the material at any point in time. This is calculated as the average of the forces within the incident and transmission bars:

$$F = \frac{1}{2} [A_{IB} E_{IB} (\epsilon_I + \epsilon_R) A_{TB} E_{TB} \epsilon_T] \tag{1}$$

Table 1 SHPB experimental parameters.

	N4000	N5100
L_{IB}	1.83 m (6')	1.82 m (6')
L_{TB}	1.83 m (6')	1.82 m (6')
D_{IB}	0.0254 m (1")	0.0191 m (3/4")
D_{TB}	0.0254 m (1")	0.0191 m (3/4")
L_{SG-1}	0.92 m (3')	0.91 m (3')
L_{SG-2}	0.92 m (3')	0.91 m (3')
E	68.9 GPa	68.9 GPa
ρ	2700 kg/m ³	2700 kg/m ³
$C_{0,IB, exp}$	5020 m/s	4998 m/s
$C_{0,TB,exp}$	4940 m/s	4957 m/s
D_{SB}	0.0191 m (3/4")	0.0191 m (3/4")
L_{SB}	0.102 m (4")	0.127 m (5")

where A represents the bar cross-sectional area and ϵ_I , ϵ_R , and ϵ_T are the incident, reflected and transmitted pulses obtained from the strain gage signals. The gap closing speed is defined in [1] as the difference between the incident bar end particle velocity, \dot{U}_1 , and the transmission bar end particle velocity, \dot{U}_2 , (Eq. (2)).

$$\dot{U} = \dot{U}_1 - \dot{U}_2 = C_{0,IB}(-\epsilon_I + \epsilon_R) + C_{0,IB}\epsilon_T \tag{2}$$

For solid specimens, the “strain rate” within the specimen is defined as \dot{U} divided by the initial specimen thickness (H_S). In this paper the same terminology is used with the understanding that, in the scope of fluid behavior, this interpretation is enhanced. We therefore have:

$$\dot{\epsilon} = \frac{\dot{U}_1 - \dot{U}_2}{H_S} = \frac{C_{0,IB}(-\epsilon_I + \epsilon_R) + C_{0,IB}\epsilon_T}{H_S} \tag{3}$$

The “strain” (ϵ) is determined by integrating Eq. (3). This is used to determine the change in specimen thickness as a function of time in Eq. (4).

$$h = H_S(1 - \epsilon) \tag{4}$$

In addition, the average axial stress applied to the fluid specimen is defined in Eq. (5) where A_B represents the bar cross-sectional area and A_S represents the specimen cross-sectional area. In the case of these experiments, the two quantities are the same.

$$\sigma = \frac{A_B E_B}{2A_S} (\epsilon_I + \epsilon_R + \epsilon_T) \tag{5}$$

Fig. 5 shows the nomenclature and coordinate system used in the vicinity of the bar–specimen interfaces. Conditions of applicability of the classic SHPB data reduction above (Eqs. (1)–(5)) were considered by Kolsky [12] and revised later by Lopatnikov et al. [13]. It is shown that the following conditions must be satisfied:

- Experiments must yield a strong transmitted signal.
- Fluid undergoes stable, laminar flow.
- The fluid specimen must be in force equilibrium.

Let us begin with the first item, as this requires the least discussion. The specimen–bar impedance ratio does not exceed 0.05 for this setup; however, it is shown in Fig. 6 that, through our choice of specimen geometry, material and testing parameters, a strong transmitted signal is achieved.

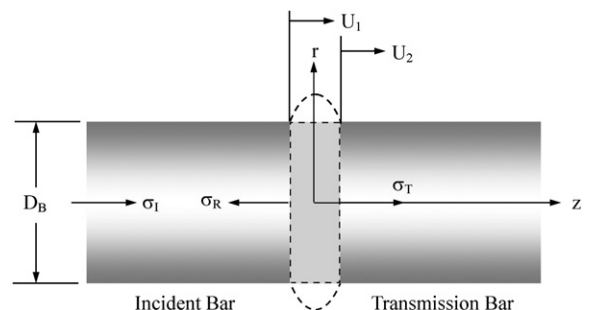


Fig. 5. SHPB diagram for bar analysis, adapted from [1].

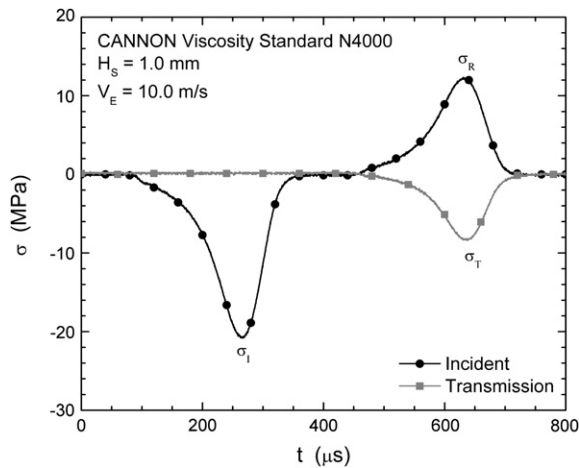


Fig. 6. Incident and transmission bar signals.

Thus, we are able to satisfy this condition and our signals can be accurately measured using our instrumentation.

A second consideration for dynamic squeeze flow is related to the stability of the fluid during the experiment. It is possible to show quantitatively that the fluid specimen undergoes stable laminar flow by calculating the Reynolds number characteristic of these experiments. The maximum velocity (\dot{U}) for these experiments is 2.0 m/s. From Eq. (22), we can determine the maximum radial velocity (at $z = h/2$) to be 19.05 m/s and 28.58 m/s for the N4000 and N5100 specimens, respectively. It follows that the maximum Reynolds numbers for these experiments are 1.7 (N4000) and 0.98 (N5100). The accepted Reynolds number below which stable, laminar flow occurs for Poiseuille flow between parallel plates is ~ 2000 [14]. These experiments fall 3 orders of magnitude below this limit and one can conclude that stable laminar flow exists during testing conducted in this study.

Achieving force equilibrium can be shown using the measured response from the strain gages during testing. Sample experimental results for a single test on a 1 mm thick N4000 fluid specimen are presented. The strain gage data in Fig. 6 depicts the incident, reflected and transmitted pulses from the first loading cycle of the CANNON N4000 viscosity standard specimen. The data was sampled at 0.2 μ s intervals (5 MHz) and was dispersion corrected using a program based on the guidelines set by Li and Lambros [15]. A complete description of the program is presented by Gama [11]. This program corrects for variations in the sound speed of the IB and TB using calibration test data, performs a Fourier transform on the data to eliminate high frequency oscillations, and sets time equal to zero at the instant the specimen experiences the incident pulse. The resulting dispersion corrected data is plotted in Fig. 7. For bars and specimens of equal cross-sectional area, the R value physically represents the net force acting on the specimen by the incident bar (i.e. the sum of the incident and reflected pulses) and the force acting on the transmitted bar (i.e. the transmitted pulse). The R value is defined as the force difference normalized by the average force. When this value approaches zero, this is an

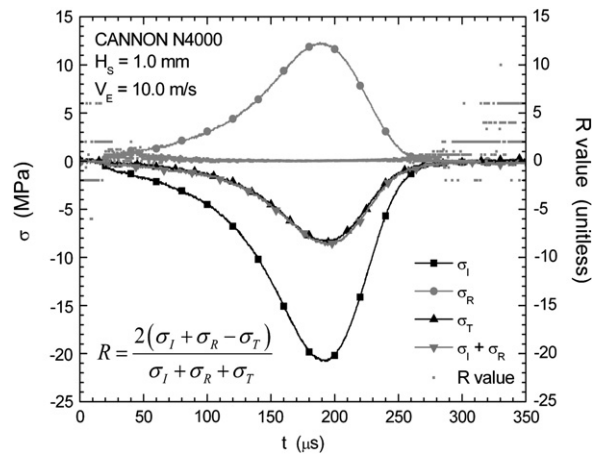


Fig. 7. Dispersion corrected data.

indication that the specimen is in force equilibrium during this loading cycle [9]. The R value is plotted in Fig. 7 for the duration of the test presented in Fig. 6.

This criterion has been met for each experiment presented in this paper. At this point, it is necessary to discuss the dynamic behavior of a viscous fluid in more detail.

5. Dynamic behavior of a viscous fluid

While the conditions of achieving force equilibrium in the timescale associated with the stress wave propagation through the specimen have been established experimentally, there are additional squeeze flow requirements which must be met. As will be shown below, a dynamic squeeze flow model including inertial terms is derived to relate the data collected during the test to the fluid viscosity. The model assumes that the flow and pressure profiles are fully developed.

In order for a fluid specimen to achieve these conditions during dynamic testing, the times required for these processes to occur must be small compared with the characteristic time of the experiment (ϵ^{-1}). In the following sections, an estimate of these characteristic times is developed. It will be shown that these estimates provide guidelines for selecting appropriate SHPB test conditions as well as specimen design, where the thickness or the diameter of the specimen can be chosen as a function of the fluid viscosity to ensure the model assumptions are valid. This methodology also establishes the limits of applicability for valid dynamic characterization of viscous fluids. In the following section, characteristic times are considered for axial wave propagation, flow and pressure development. It is recognized that these responses can occur simultaneously but as a first step they are treated individually using analytical estimates. When available, our estimates are compared to expressions extracted from previous work.

5.1. Axial wave propagation

During a SHPB test, the viscous fluid specimen will respond in several ways. First, the stress wave in the

incident bar will travel through the specimen thickness to the transmission bar. The specimen can be considered to be in stress equilibrium through the thickness depending on the specimen thickness and wave speed (Fig. 8).

Given the thickness and actual sound speed (752–1009 m/s from [9]) of the N4000 fluid specimen, it is possible to estimate the time required for the stress wave to traverse the specimen (Eq. (6)).

$$\tau_H = \frac{H_S}{C_0} \tag{6}$$

Since the specimens discussed in this work are very thin (0.5–1.0 mm), this time will be very small (on the order of 1 μ s) compared with the timescale of each experiment. Hence, the specimen can be considered to be in local force equilibrium across its thickness, even when considering multiple reverberations. This is consistent with the measured forces across the bar diameter shown in Fig. 7. Just this fact alone defines the applicability of the classic SHPB approach and data reduction to these viscous fluids. The effect of specimen thickness on equilibrium development has been evaluated and discussed specifically by Song and Chen in [16]. Additional information is provided in [17–19].

5.2. Pressure profile development

The second process to be considered is the development of the pressure profile across the radius of the fluid specimen. Due to the pressure gradient between the center and outer boundary of the specimen (i.e. zero pressure), a non-uniform pressure profile will develop across the specimen radius. This progression is illustrated in Fig. 9. At $t=0$, a constant pressure profile exists across the radius. This profile will develop into a linear pressure profile over the radius that is constant in the thickness direction (it will be shown that the axial wave propagation occurs much more rapidly than the time for pressure profile development). An estimate of this characteristic time is derived next.

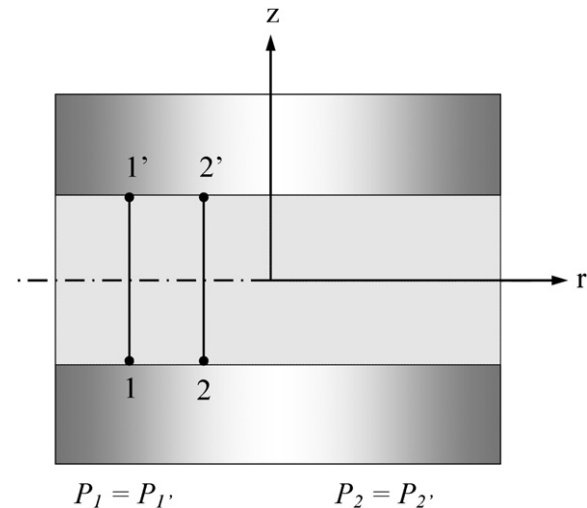


Fig. 8. After a short time, τ_H , the pressure across the fluid layer reaches equilibrium.

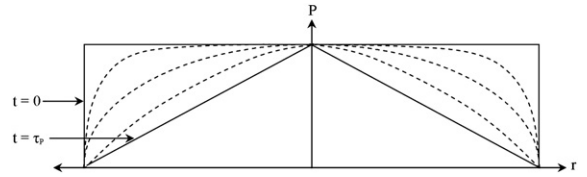


Fig. 9. Pressure profile development across the specimen radius.

In the case of a viscous fluid in a narrow gap ($R > h$), the viscosity can strongly affect the pressure profile development time. This time is determined by first writing the continuity equation for a compressible fluid in which there is no source or sink of mass, where V_r and V_z represent the fluid velocities in the r and z directions:

$$\frac{\partial \rho}{\partial t} + \rho \left(\frac{1}{r} \frac{\partial (rV_r)}{\partial r} + \frac{\partial V_z}{\partial z} \right) = 0 \tag{7}$$

We can make the approximation:

$$\frac{\partial V_z}{\partial z} \approx \frac{\dot{U}_1 - \dot{U}_2}{h} = \dot{\epsilon}(t) \tag{8}$$

Here \dot{U}_1 and \dot{U}_2 represent the velocity of the transmitter and incident bar surfaces, respectively, and $\dot{\epsilon}(t)$ represents the current strain rate. Considering only cylindrically symmetric flow in the r -direction, it is possible to rewrite the continuity equation:

$$\frac{\partial \rho}{\partial t} + \rho \frac{1}{r} \frac{\partial (rV_r)}{\partial r} = \rho \dot{\epsilon}(t) \tag{9}$$

Now it is necessary to consider the momentum balance equation in the r -direction to obtain a relationship between V_r and ΔP . Additional assumptions inherent in Eq. (10) are no slip between the bar and fluid and zero body forces:

$$\rho \frac{\partial V_r}{\partial t} = -\frac{\partial P}{\partial r} + \mu \frac{\partial^2 V_r}{\partial z^2} \tag{10}$$

Here, it is possible to make the approximation:

$$\frac{\partial^2 V_r}{\partial z^2} \approx -\frac{V_r}{H_S^2} \tag{11}$$

Neglecting the transient inertial term, which is small in comparison to the gradient of pressure, yields a ‘‘Darcy’s law’’ for the gap:

$$\frac{\partial P}{\partial r} + \frac{\mu}{H_S^2} V_r = 0 \tag{12}$$

The coefficient, μ/H_S^2 , represents the permeability of the gap for a viscous fluid. Eq. (12) can be solved for the fluid velocity in the r -direction:

$$V_r = -\frac{H_S^2}{\mu} \frac{\partial P}{\partial r} \tag{13}$$

This can now be substituted back into Eq. (9) to yield Eq. (14), where ν represents the kinematic viscosity of the fluid.

$$\frac{\partial \rho}{\partial t} - \frac{H_S^2}{\nu} \frac{1}{r} \frac{\partial}{\partial r} \left(r \frac{\partial P}{\partial r} \right) = -\rho \dot{\epsilon} \tag{14}$$

The pressure change and density in the fluid can be expressed as $\Delta P = -K_f \varepsilon$ and $\rho = \rho_0(1 - \varepsilon)$, where K_f is the bulk modulus of the fluid and ρ_0 is its initial density. Combining these expressions yields: $\Delta \rho = \Delta P / C_0^2$, where $C_0 = \sqrt{K_f / \rho_0}$ and $\Delta \rho = \rho - \rho_0$. Substituting this relationship into Eq. (14) yields:

$$\frac{\partial P}{\partial t} - \frac{H_s^2 C_0^2}{\nu} \frac{1}{r} \frac{\partial}{\partial r} \left(r \frac{\partial P}{\partial r} \right) = -\rho C_0^2 \dot{\varepsilon} \quad (15)$$

Eq. (15) represents a diffusion equation known as the equation of piezoconductivity [20] with an effective diffusion coefficient, $D_p = H_s^2 C_0^2 / \nu$, written here for a specimen with cylindrical symmetry. A similar expression has been derived by Basov et al. [20] describing the behavior of a power law fluid under oscillatory flow using Cartesian coordinates. This equation describes the *diffusion of pressure* related with the viscous resistance of the fluid to flow. Thus, the characteristic time required for pressure profile development from an initial constant pressure to a linear profile can be described by this characteristic time related with the viscous piezoconductivity of the gap (Eq. (16)).

$$\tau_p \approx \frac{R^2}{D_p} = \frac{\nu R^2}{C_0^2 H_s^2} \quad (16)$$

Eq. (16) includes the effects of material properties and specimen geometry on this characteristic time. Hence, this expression provides guidance on selection of bar diameter and specimen thickness as a function of kinematic viscosity. Another reference time for pressure profile development can be related to the time for a wave to propagate across the radius of the specimen:

$$\tau_R = \frac{R}{C_0} \quad (17)$$

It is shown in a later section that this time can become important for fluids of low viscosity. Both of these parameters are useful for defining the limits of valid SHPB test conditions.

5.3. Flow profile development

The third dynamic process which must be addressed is the development of the stationary parabolic flow profile of radial velocity. This process is related with the development of viscous boundary layers near the bar walls. With time, these boundary layers overlap and form a parabolic profile (Fig. 10).

A conservative estimate of this characteristic time is given by the time required for a viscous wave to travel through the specimen thickness,

$$\tau_V = \frac{H_s}{c_v} \quad (18)$$

Here, the speed of the transverse shear wave is given by c_v , which has been defined by Wilhelm and Hong [21] as the shear wave speed in an infinite fluid (Eq. (19)).

$$c_v = (\nu / \tau_V)^{1/2} \quad (19)$$

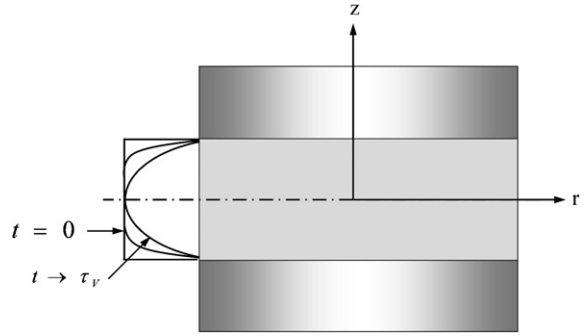


Fig. 10. Flow profile development.

τ_V is a general relaxation time. For our situation, we define this as the time required for the wave to travel through the specimen thickness (Eq. (18)). Combining Eqs. (18) and (19) results in an expression describing the characteristic time for flow profile development:

$$\tau_V \approx \frac{H_s^2}{\nu} \quad (20)$$

Let us now use these characteristic times to develop a criterion for specimen design. For a valid SHPB test, the duration of the loading pulse must be greater than the maxima in the four characteristic times discussed above (axial and radial wave travel times and pressure and flow development times). In Fig. 11, the characteristic times for a 1.0 mm thick, 25.4 mm diameter specimen are plotted as a function of the fluid kinematic viscosity. Based on Eq. (20), the velocity profile development time decreases with increasing viscosity, while the pressure profile characteristic time increases (see Eq. (16)). In this plot, it is clear that, for a N4000 viscosity standard ($\nu = 20,000 \text{ mm}^2/\text{s}$) specimen with the above geometry, the governing characteristic time is the flow development time of $50 \mu\text{s}$. In this regime, one also notes that the time for pressure development is governed by the travel time in the radial direction ($\tau_R > \tau_p$). Physically speaking, the pressure development across the specimen radius will not occur faster than the time it takes

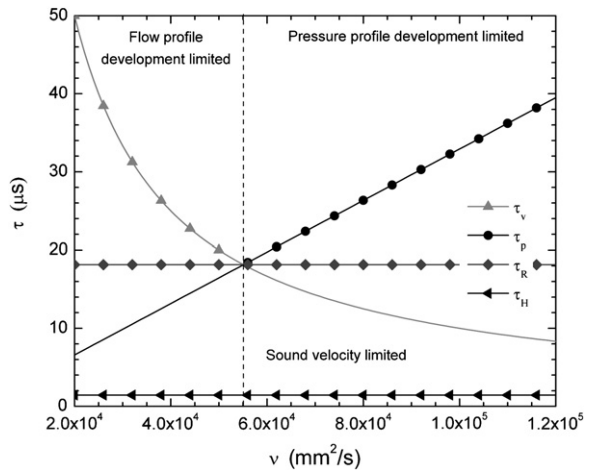


Fig. 11. Characteristic equilibrium times for dynamic processes for a 1.0 mm specimen.

sound to travel that distance. However, for materials with a kinematic viscosity higher than 55,000 mm²/s, the process becomes piezo-conductivity dominated where the governing characteristic time is now the pressure development time.

From Fig. 11, it is clear that, for a given fluid kinematic viscosity, there is a specific specimen geometry at which the flow and pressure profile characteristic times reach a minimum. This triple point can be expressed by the relationship:

$$\frac{R}{H_S} \frac{\nu}{C_0} = 1 \tag{21}$$

Eq. (21) allows one to select a specimen aspect ratio (R/H_S) which will result in the lowest possible governing characteristic time for a given material (and hence the triple point represents the highest strain rate that can be tested without violating the assumptions of the squeeze flow model developed in the next section). This procedure is illustrated in a later section for the case of the N5100 fluid.

In our experiments on N4000, the specimen radius was limited by the available bar diameter and the smallest possible specimen thickness was used in order to yield a strong transmitted pulse. As a result, these specimens have a higher flow characteristic time (as stated above) than the pressure characteristic time.

6. Squeeze flow model

Given that all characteristic times are satisfied, a dynamic squeeze flow model including inertial forces can be used to describe the SHPB experiment for a fluid specimen. The classic squeezing flow model developed by Stefan [22] has been modified to include terms accounting for the fluid inertia by Kuzma [23] and is written in Eq. (23) along with the radial flow velocity (Eq. (22)) and shear rate (Eq. (24)).

$$V_r = \frac{3r}{h^3}(z^2 - hz)(\dot{U}_1 - \dot{U}_2) \tag{22}$$

$$F = \frac{\pi R^4}{4} \left(\underbrace{\frac{3\rho}{5h}(\dot{U}_1 - \dot{U}_2)}_{\text{transient inertial}} + \underbrace{\frac{15\rho}{14h^2}(\dot{U}_1 - \dot{U}_2)^2}_{\text{bulk inertial}} + \underbrace{\frac{6\mu}{h^3}(\dot{U}_1 - \dot{U}_2)}_{\text{viscous}} \right) \tag{23}$$

$$\dot{\gamma}_{rz} = \frac{\partial V_r}{\partial z} + \frac{\partial V_z}{\partial r} = -\frac{6rz}{h^3}(\dot{U}_1 - \dot{U}_2) \tag{24}$$

The experimental force, F , is determined from the bar strain measurements using Eq (1). The transient and bulk inertial terms are calculated from geometry, fluid density and experimental measurements of the bar end velocities (Eq. (2)) and accelerations. Bar end accelerations are calculated by taking the time derivative of locally smoothed bar end velocity curves at each point in time. The instantaneous thickness is determined according to Eq. (4).

Now, these inertial terms may be subtracted from the experimentally measured force, leaving only the experimental viscous force contribution. In Eq. (25), the slope of the curve is the fluid viscosity of interest.

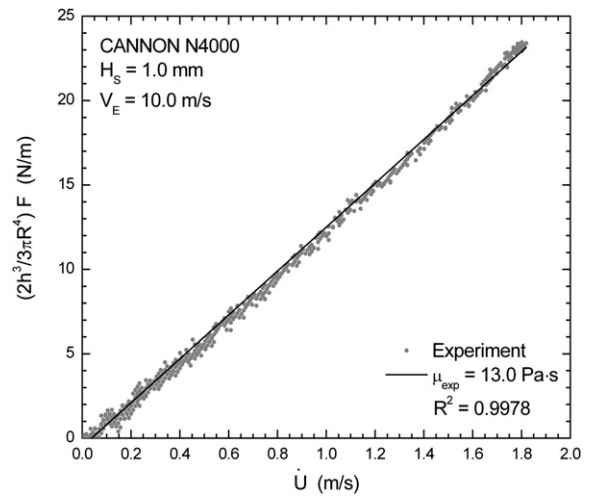


Fig. 12. Determining viscosity using the quasi-static squeeze flow theory for a N4000 fluid specimen.

$$\frac{2h^3}{3\pi R^4} F_{v,exp} = \mu_{exp} \dot{U} \tag{25}$$

For information on the squeezing flow behavior of non-Newtonian materials, the review paper by Engmann et al. [24] is a good resource.

7. Theory–experiment correlation

Let us now examine the accuracy of the quasi-static squeeze flow model predictions for SHPB experimental data taken using the 1.0 mm thick, 25.4 mm diameter N4000 fluid specimen discussed previously with a maximum characteristic time of $\tau_V = 50 \mu s$. The pressure profile development time for this material is governed by the sound travel time across the specimen radius ($\tau_R = 18.1 \mu s$), which is small compared with the typical duration of the test (275 μs). A linear relationship is found for the loading portion of all tests consistent with Eq. (25).

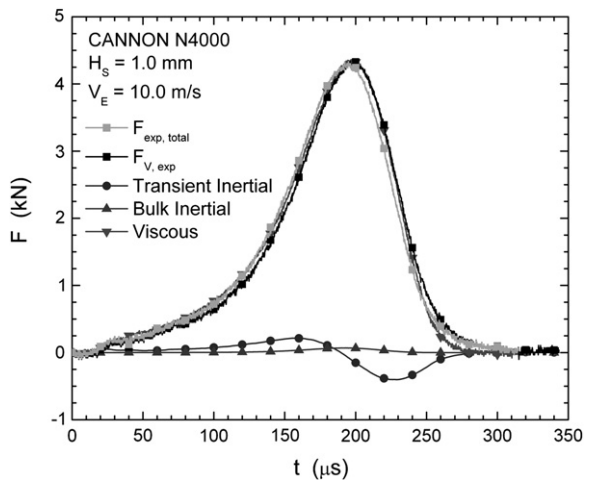


Fig. 13. Theoretical prediction using the viscosity determined in Fig. 12 plotted against the viscous experimental force.

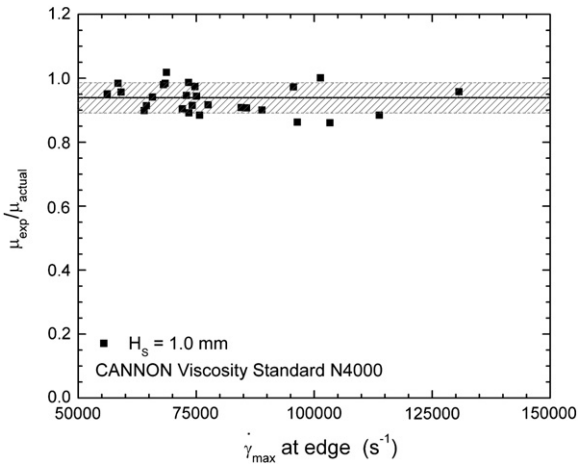


Fig. 14. Normalized viscosity plotted against max shear rate for N4000 standard specimens.

Given the cubic dependence on specimen thickness and the fact that thickness varies continuously with time during the test, this linear correlation provides convincing evidence that our approach is accurately capturing the correct physics for dynamic squeeze flow. A typical result is shown in Fig. 12 where the fluid viscosity is found to be 13.0 Pa s with a correlation coefficient of 0.9978. Using this value, excellent correlation is shown in Fig. 13 between the model prediction and experiments for the transient viscous force during loading and unloading of the specimen.

The viscosity is normalized using the actual viscosity (μ_{actual}) of the standard at the experimental temperature (Fig. 4). The normalized viscosities from 25 experiments have been plotted in Fig. 14 according to the maximum shear rate at the specimen edge defined in Eq. (24) in each experiment. These experiments are performed at low enough rates that the isothermal testing requirement is satisfied and the specimen characteristic times do not exceed the characteristic experimental timescale. When the specimen design criteria are satisfied, good

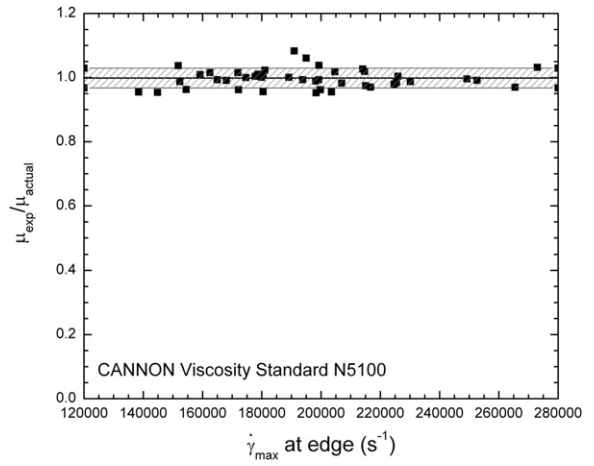


Fig. 16. Normalized viscosity plotted against max shear rate for N5100 fluid specimens.

agreement ($\mu_{exp}/\mu_{actual} = 0.94 \pm 0.05$) was achieved over a wide range of maximum shear rates at the specimen edge (50,000–150,000 s^{-1}).

To complete the experimental study, the N5100 viscosity standard was evaluated under the ideal specimen design conditions (i.e. triple point) shown in Fig. 15 ($\tau_p = \tau_v = \tau_R = 13.6 \mu s$). With a kinematic viscosity of 18,500 mm^2/s , the N5100 fluid specimen meets the requirements for minimal profile development times for 19.05 mm diameter, 0.5 mm thick specimens. The average loading time for these experiments is 200 μs . For these specimens, the theory–experiment correlation is plotted in Fig. 16, where an excellent match is seen ($\mu_{exp}/\mu_{actual} = 1.00 \pm 0.03$). The maximum axial strain rate achievable for this configuration should be limited to 7350 s^{-1} (shear strain rate of 382,000 s^{-1}) in accordance with the guidelines established in this study.

These results prove the concept of SHPB testing for thin viscous fluids; reasonable data corresponding with the known rheological behavior of the N4000 and N5100 fluid specimens has been obtained. A good understanding of the effect of dynamic processes on experimental results for SHPB testing is demonstrated herein. With suitable specimen design, accurate measurements of viscosity can be obtained.

8. Conclusions

The requirements for a valid SHPB test of a viscous Newtonian fluid specimen are discussed in detail. The classic Kolsky data reduction method is presented along with the conditions under which this method may be applied. Characteristic timescales for four dynamic processes have been determined, each as a function of material properties and specimen geometry. Using this knowledge, the criterion in Eq. (21) was developed, which allows one to determine the ideal specimen geometry (radius and gap) for a material of known sound velocity and kinematic viscosity. In cases where these are unknown, estimates may be used to provide a range of feasible specimen geometries.

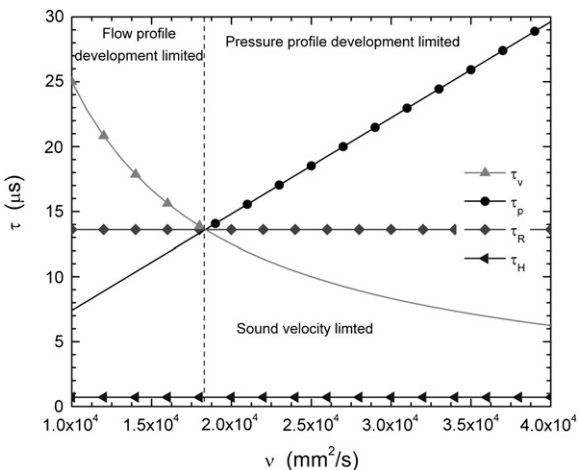


Fig. 15. Characteristic equilibration times for a 0.5 mm thick, 19.05 mm diameter specimen.

A squeeze flow model including inertial forces has been experimentally validated using model Newtonian fluids. The model accurately predicts the transient force applied to the specimen during SPHB testing. Specimen viscosities have been measured at shear strain rates up to $280,000 \text{ s}^{-1}$ and are found to be in excellent agreement with the known viscosity when the test methodology is satisfied. Viscous heating of the specimens is found to be negligible for the testing conditions investigated in this paper. For higher rates or more viscous materials, it will be necessary to account for this in temperature-sensitive materials.

Acknowledgement

The authors would like to acknowledge Norman J. Wagner, Ph.D. (University of Delaware Department of Chemical Engineering), Eric D. Wetzel, Ph.D. (Army Research Laboratory), Bazle A. Gama, Ph.D., Joseph M. Deitzel, Ph.D. (University of Delaware Center for Composite Materials), David M. Stepp (Army Research Office) and Caroline H. Nam, Ph.D. (University of Delaware Department of Chemical Engineering) for their helpful discussions and contributions to this research, as well as Dennis Kalman (University of Delaware Department of Chemical Engineering) for his assistance in acquiring the rheological data in Figs. 1 and 2. Nick Waite (University of Delaware Department of Electrical Engineering) has also contributed greatly to the development of the current SHPB experimental setup.

Research was sponsored by the U.S. Army Research Office and U.S. Army Research Laboratory and was accomplished under Cooperative Agreement Number #W911NF-05-2-0006. The views and conclusions contained in this document are those of the authors and should not be interpreted as representing the official policies, either expressed or implied, of the Army Research Office, Army Research Laboratory, or the U.S. Government. The U. S. Government is authorized to reproduce and distribute reprints for Government purposes notwithstanding any copyright notation hereon.

References

- [1] B. Gama, S. Lopatnikov, J. Gillespie Jr., Hopkinson bar experimental technique: a critical review, *Applied Mechanics Review* 57 (4) (2004) 223–250.
- [2] C. Macosko, *Rheology: Principles, Measurements, and Applications*, Wiley-VCH, Inc., 1994.
- [3] Y. Lee, N. Wagner, Rheological properties and small-angle neutron scattering of a shear thickening, nanoparticle dispersion at high shear rates, *Industrial and Engineering Chemical Research* 45 (2006) 7015–7024.
- [4] V. Kenner, The fluid Hopkinson bar, *Experimental Mechanics* 20 (7) (1980) 226–232.
- [5] E. Hoglund, R. Larsson, Modeling non-steady EHL with focus on lubricant density, *Elastohydrodynamics* (1996) 511–521.
- [6] B. Åhrström, S. Lindqvist, E. Höglund, K. Sundin, Proceedings of the Institution of Mechanical Engineers Part J – Journal of Engineering Tribology (2002) 63–73.
- [7] S. Clyens, C. Evans, K. Johnson, Measurement of the viscosity of supercooled liquids at high shear rates with a Hopkinson torsion bar, *Proceedings of the Royal Society of London. Series A* 381 (1982) 195–214.
- [8] K. Ogawa, Dynamic behavior of viscous fluid at high rate of shear using through bar method, *Journal of Physics IV France* 110 (2003) 435–440.
- [9] B. Krentsel, B. Kleiner, L. Stoykaya, *Visshiy Polyolefyny. (High-molecular Polyolefins)* (1984) Moscow (In Russian).
- [10] G. Grey III, Classic split-Hopkinson pressure bar testing, *Mechanical Testing and Evaluation*, In: *ASM Handbook*, vol. 8 (2000) pp. 488–496.
- [11] B. Gama, *Split Hopkinson Pressure Bar Technique: Experiments, Analyses and Applications*, University of Delaware, Newark, 2004.
- [12] H. Kolsky, An investigation of the mechanical properties of materials at very high rates of loading, *Proceedings of the Physical Society* 62 (II-B) (1949) 676–700.
- [13] S. Lopatnikov, B. Gama, C. Krauthauser, J. Gillespie Jr., Applicability of the classical analysis of experiments with split Hopkinson pressure bar, *Technical Physics Letters* 30 (2004) 102–105.
- [14] J. Walker, G. Whan, R. Rothfus, Fluid friction in noncircular ducts, *AIChE Journal* 3 (4) (1957) 484–489.
- [15] W. Li, J. Lambros, Determination of the dynamic response of brittle composites by the use of the split Hopkinson pressure bar, *Experimental Mechanics* 59 (7) (1999) 1097–1107.
- [16] B. Song, W. Chen, Dynamic stress equilibration in split Hopkinson pressure bar tests on soft materials, *Experimental Mechanics* 44 (3) (2004) 300–312.
- [17] G. Gray III, W. Blumenthal, Split-Hopkinson pressure bar testing of soft materials, *Mechanical Testing and Evaluation*, In: *ASM Handbook*, vol. 8 (2000) 488–496.
- [18] W. Chen, B. Song, D. Frew, M. Forrestal, Recent developments in split Hopkinson pressure bar testing, *Ceramic Transactions* 134 (2002) 217–224.
- [19] B. Song, W. Chen, Z. Liu, S. Erhan, Compressive properties of soybean oil-based polymers at quasi-static and dynamic strain rates, *Journal of Applied Polymer Science* 99 (2005) 2759–2770.
- [20] N. Basov, A. Leonov, S. Lyubartovich, I. Felipchuk, Propagation of large-amplitude low-frequency vibrations in polymer melt flows, *Mechanics of Composite Materials* 10 (3) (1974) 444–451.
- [21] H. Wilhelm, S. Hong, Stress relaxation waves in fluids, *Physical Review A* 22 (3) (1980) 1266–1271.
- [22] J. Stefan, Versuche über die scheinbare Adhäsion, *Sitz Kais Akad Wiss Math Nat Wien* 69 (2) (1874) 713–735.
- [23] D. Kuzma, Fluid inertia effects in squeeze films, *Applied Science Research* 18 (1967) 15–20.
- [24] J. Engmann, C. Servais, A. Burbidge, Squeeze flow theory and applications to rheometry: a review, *Journal of Non-Newtonian Fluid Mechanics* 132 (2005) 1–27.